Monsoon-Frontal Interactions Drive Cyclone Biparjoy's Wake Recovery in the Arabian Sea

Siddhant Kerhalkar[1], Ankitha Kannad[2], Alex Kinsella[3], Amit Tandon[1,4], Janet Sprintall[2], Craig M. Lee[5]

[1]School for Marine Science and Technology, University of Massachusetts Dartmouth, New Bedford, MA, USA
[2]Scripps Institution of Oceanography, University of California, San Diego, La Jolla, CA, USA
[3]Department of Physical Oceanography, Woods Hole Oceanographic Institution, Woods Hole, MA, USA
[4]Mechanical Engineering Department, University of Massachusetts Dartmouth, North Dartmouth, MA, USA
[5]Applied Physics Laboratory, University of Washington, Seattle, WA, USA

Key Points:

- Slow moving cyclone Biparjoy in the Arabian Sea triggers the formation of a cold, salty and productive wake, causing a 4 °C drop in SSTs.
- In-situ observations reveal the asymmetric recovery of the cold wake, with differences in mixed layer depth and buoyancy gradients at edges.
- Interaction of winds with wake filament shows signatures of submesoscale processes, underscoring their role in the wake's recovery.

Corresponding author: Amit Tandon, atandon@umassd.edu

Abstract

Cold wakes generated by cyclones enhance productivity and impact the local air-sea interaction, paths and intensities of subsequent storms in the region. However, in-situ observations of the recovery across such wakes are rare. A cold wake in the Arabian Sea was surveyed using multiple ship-board instruments approximately 10 days after the passage of Cyclone Biparjoy in 2023. The wake, nearly 30 km wide, had a stronger (weaker) buoyancy gradient at its eastern (western) edge and assumed a upfront (downfront) orientation relative to the south-westerly monsoon winds. This resulted in notable asymmetry in vertical temperature, salinity and velocity structures at the edges of the wake. While the wake recovery following a cyclone is often attributed to one-dimensional diurnal heating and cooling process, these observations underscore the role of coupling of monsoon winds and the underlying three-dimensional submesoscale fronts in speeding the recovery of a slow-moving cyclone through various submesocale processes.

Plain Language Summary

Tropical cyclones create cold wake trail of water mixed upward from deeper waters, but observations of recovery of the wake back to pre-cyclone conditions are rare. These wakes play a crucial role to modulate availability of nutrients in the ocean, impact local atmosphere-ocean interaction and future passage of storms in the region. This study describes the structure of this trail and processes associated with its recovery after slow-moving Cyclone Biparjoy in the Arabian Sea in 2023. Our observations reveal that the wake is asymmetrical in its density and velocity structure. This is a result of the interaction between monsoon winds from the south-west and the density differences at the edges of the wake. Alongside the daily cycle of heating and cooling, these interactions foster small-scale three-dimensional processes, that are found to be crucial for the cold wake recovery back toward typical pre-cyclone conditions.

1 Introduction

Tropical cyclones, known for their high wind speeds, create a cold (and sometimes salty) wake due to increased vertical mixing, causing sea surface temperatures (SSTs) within the wake to drop by 2 °C to 4 °C (Stramma et al., 1986). However, this wake forms asymmetrically relative to the cyclone track, usually to the right of the cyclone eye in the Northern Hemisphere due to wind stress configurations (Price, 1981; Cornillon et al., 1987; Sanabia & Jayne, 2020). While the cold wake's formation as a result of enhanced turbulent mixing is well understood (D'Asaro, 2003; Emanuel, 2003; D'Asaro et al., 2007; Vincent et al., 2012), its recovery back to pre-cyclone conditions has received less attention. Understanding the evolution of the cold wake and its recovery is critical as it can significantly impact ocean heat transport, and the predictability of the path and intensity of subsequent storm systems that traverse the region (Emanuel, 2001; Pasquero & Emanuel, 2008; Karnauskas et al., 2021; Gutiérrez Brizuela et al., 2023). Significantly, tropical cyclones are often considered as the signature of the onset of Asian Monsoons, and hence, the cyclone wake conditions can impact sub-seasonal predictions of monsoons (Krishnamurti et al., 1981; Evan & Camargo, 2011; Krishnamurti et al., 2007).

Initial hypotheses suggested atmospheric surface forcing causes a wake recovery over 10 days or more (Price et al., 2008), but subsequent observational studies demonstrated that background advection also played a major role in the recovery of the cold wake (Mrvaljevic et al., 2013; Johnston et al., 2020). Numerical modeling results indicate that baroclinic instabilities at the edges of the cold wake lead to the formation of submesoscale mixed-layer eddies, leading to restratification and contributing to the wake's recovery (Fox-Kemper et al., 2008; Haney et al., 2012; Mei & Pasquero, 2012; Smith et al., 2019; Yi et al., 2024). Additionally, winds blowing parallel to the fronts at the edges of the cold wake, create up-front (winds opposing the surface thermal wind shear) and downfront configurations (winds in direction of surface thermal wind shear), causing an asymmetric recovery of the wake due to Ekman buoyancy fluxes (EBFs). These recovery processes are also found to be interacting with each other (Mahadevan et al., 2010; Haney et al., 2012).

Nonetheless, in-situ observations of lateral submesoscale processes affecting the recovery of the cold wake are lacking. For example autonomous profilers such as Argo are typically not fast enough to capture the spatio-temporal evolution of the wake, even in highly networked field campaigns (e.g., D'Asaro et al., 2007; Johnston et al., 2021). While this challenge could be addressed with ship-based sampling, heightened surface waves associated with hurricanes along with other logistical obstacles render ship usage unfeasible unless the sampling strategy is critically timed, typically a few days after cyclone passage.

In this study, we utilize rare ship-based, in-situ observations conducted in the Arabian Sea during the "Enhancing Knowledge of the Arabian Sea Marine Environment through Science and Advanced Training (EKAMSAT)" program, which sample the wake of Cyclone Biparjoy in June 2023. Our goal is to document the horizontal and vertical variability in the cyclone wake and its vicinity. We first provide an overview of the instruments and satellite products used in this study (Section 2), before describing the cold wake recovery using our unique observations and demonstrating the presence of submesoscale processes in this wake recovery (Section 3). The summary of our findings and its broader implications are discussed in Section 4.

2 Data and Methods

A combination of measurements collected by a ship-mounted flow-through thermosalinograph (TSG) and an Underway CTD (uCTD) profiler were employed to investigate the temperature and salinity structures within the cold wake resulting from Tropical Cyclone Biparjoy in the Arabian Sea between 17-20 June 2023. The TSG provides measurements at the 4 m depth based on R/V Revelle's seawater intake, while the uCTD collected profiles over the top 250 m with a vertical resolution of 4 m and a temporal resolution of 10 minutes (an approximate horizontal resolution of 1.7 km). Meteorological conditions were measured from sensors housed on the ship's bow mast. The velocity structure within the cold wake was measured using the Hydrographic Doppler Sonar System (HDSS, Pinkel, 2012) over the top 550 m at a vertical resolution of 4.5 m. The mixed layer depth (MLD) is inferred from the uCTD measurements based on a 0.125 kg/m^3 density difference from surface values (Monterey & Levitus, 1997), while the isothermal layer depth (ILD) is defined based on a 0.5 °C temperature difference with respect to the surface values(Levitus, 1983). The barrier layer thickness (BLT) is the difference between the ILD and the MLD.

We also utilize various remote sensing products such as the 3-Day product from Advanced Microwave Scanning Radiometer-2 (AMSR-2, Wentz et al., 2014) and NOAA 0.25 ° Daily Optimum Interpolation Sea Surface Temperature (OISST, Reynolds et al., 2007) at a spatial resolution of nearly 25 km to examine the SSTs. Additionally, we assess the SST and chlorophyll-a from level-2 versions of Moderate-resolution Imaging Spectroradiometer (MODIS) Aqua (NASA Goddard Space Flight Center, 2018) and Visible Infrared Imaging Radiometer Suite (VIIRS) on NOAA-20 and NPP platforms, with a spatial resolution of 750 m (Cao et al., 2013).

3 Results

3.1 Remote Sensing of the Cyclone Wake Recovery

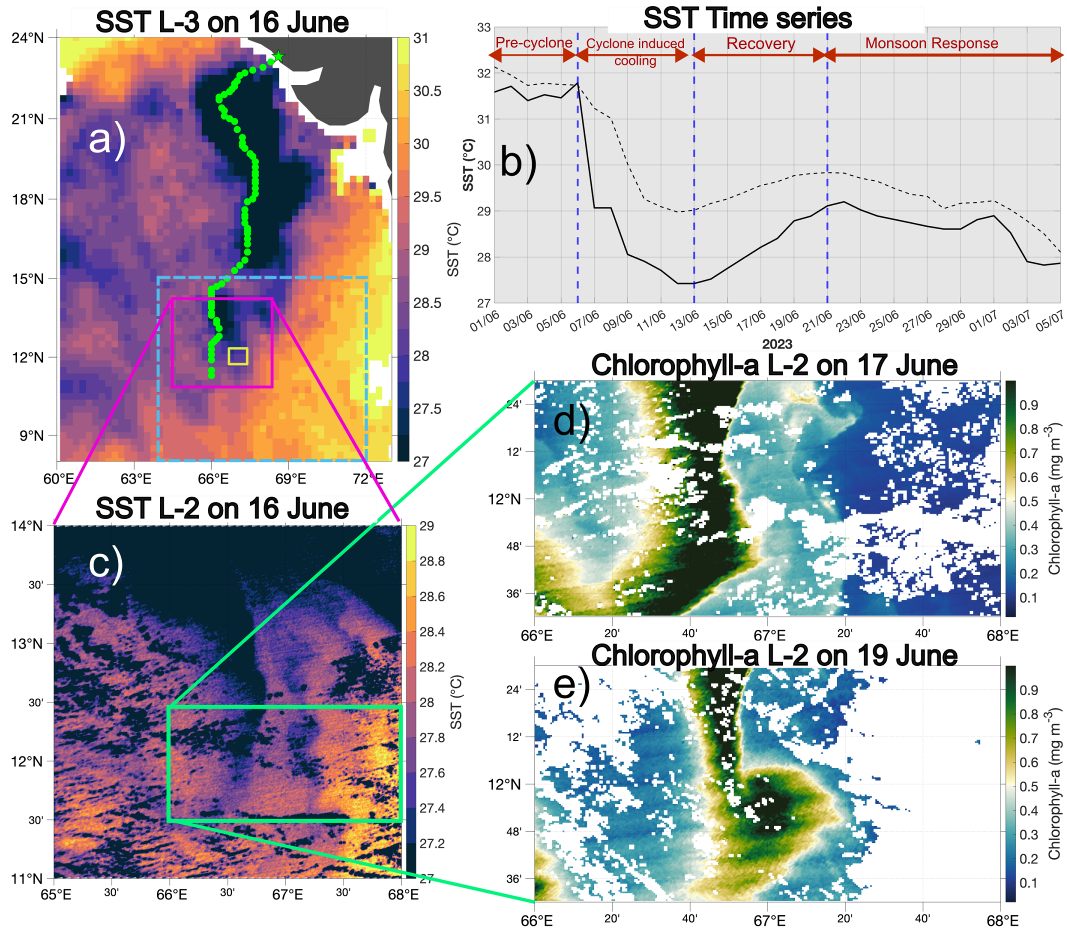

Figure 1. a) SST from AMSR-2 on 16 June 2023. The green dots indicate the path of the cyclone Biparjoy (as obtained from IMD, 2023). b) Time series of mean SSTs from AMSR-2 between 1 June and 5 July 2023. Solid line indicates the mean SST over the smaller area around the ship operations in panel a) (yellow solid box) while the dashed line indicates the same over the larger area in panel a) (dashed blue box). c) SST from MODIS Aqua L-2 product on 16 June 2023 over the solid magenta box in a). d) Chlorophyll-a from VIIRS-NPP on 17 June 2023 over the green box highlighted in c). e) The same as d) but from VIIRS-NOAA on 19 June 2023.

Cyclone Biparjoy, a slow-moving cyclone with translation speeds of 1-2 m s^{-1} (Figure S1a), formed over the southern Arabian Sea on 5 June 2023. It reached its peak intensity as a category-3 cyclone and moved northward before making landfall over Gujarat, India on 15 June (IMD, 2023). Cyclone propagation resulted in the formation of the cold wake predominantly to the right of the track (Figure 1a), with a 4 °C drop in SST over seven days (Figure 1b) at the ship's operational area (yellow box in Figure 1a).

The cyclone wake begins to recover on 13 June, which is identified by a rise in SST by 1.7 °C over eight days (Figure 1b). With wind speeds and peak shortwave radiation in the wake area around 8 $\mathrm{m\,s^{-1}}$ and 940 $\mathrm{W/m^2}$ respectively (Figure S3), the theoretical recovery period for the wake, if driven only by surface forcing, is estimated to be 18-29 days (see Supplementary Section S1, Price, 1981; Haney et al., 2012). However, the rise in SST (or the surface recovery of the wake) ceases after 8 days instead (13-21 June, Figure 1b), reaching a steady state, although it fails to return to pre-cyclone values (Figure 1b). A large region of the southeastern Arabian Sea (marked by dashed blue line in Figure 1a) exhibits a similar recovery pattern. While the large-scale forcing from the Southwest Monsoon over the Arabian Sea prevents the SST to return to pre-cyclone values, the presence of small-scale lateral processes due to the cyclone wake, such as mixed layer eddies as well as EBFs, can contribute to the ambiguities in the recovery time-scale (e.g. Haney et al., 2012).

Since the entrainment in the wake increases nutrient availability, this results in higher chlorophyll values within the wake (Babin et al., 2004). Therefore, high chlorophyll values are used as markers of cyclone wake. Thus the presence of lateral processes around the wake are inferred using the high resolution infrared L-2 images of SST and chlorophyll. The wake's meandering nature is evident with warmer SSTs at the edges and SSTs of 27.4 °C at the core of the wake (Figure 1c). Initially, the meandering front of the wake aligns in the north-south direction. However, it begins to roll up after a few days (Figure 1d,e). We next investigate the in-situ sub-surface measurements of the wake to reveal the presence of lateral processes around the wake.

3.2 In-situ survey of the wake

An in-situ survey from the ship's TSG and the uCTD system were conducted 10 days after the cyclone's passage to examine the structure of the generated wake (Figure S2, S3). The winds during this period were generally south-westerly (consistent with the direction of winds during the monsoon season, Figure S3a). These observations verify the presence beneath the ocean surface of the wake, which spans approximately 30 km in width. In the near-surface layer, the core of the wake is characterized by colder (a difference of 0.72 °C), saltier (0.45 $\mathrm{g\,kg^{-1}}$ difference) and therefore denser (a difference of 0.39 $\mathrm{kg/m^3}$) waters when

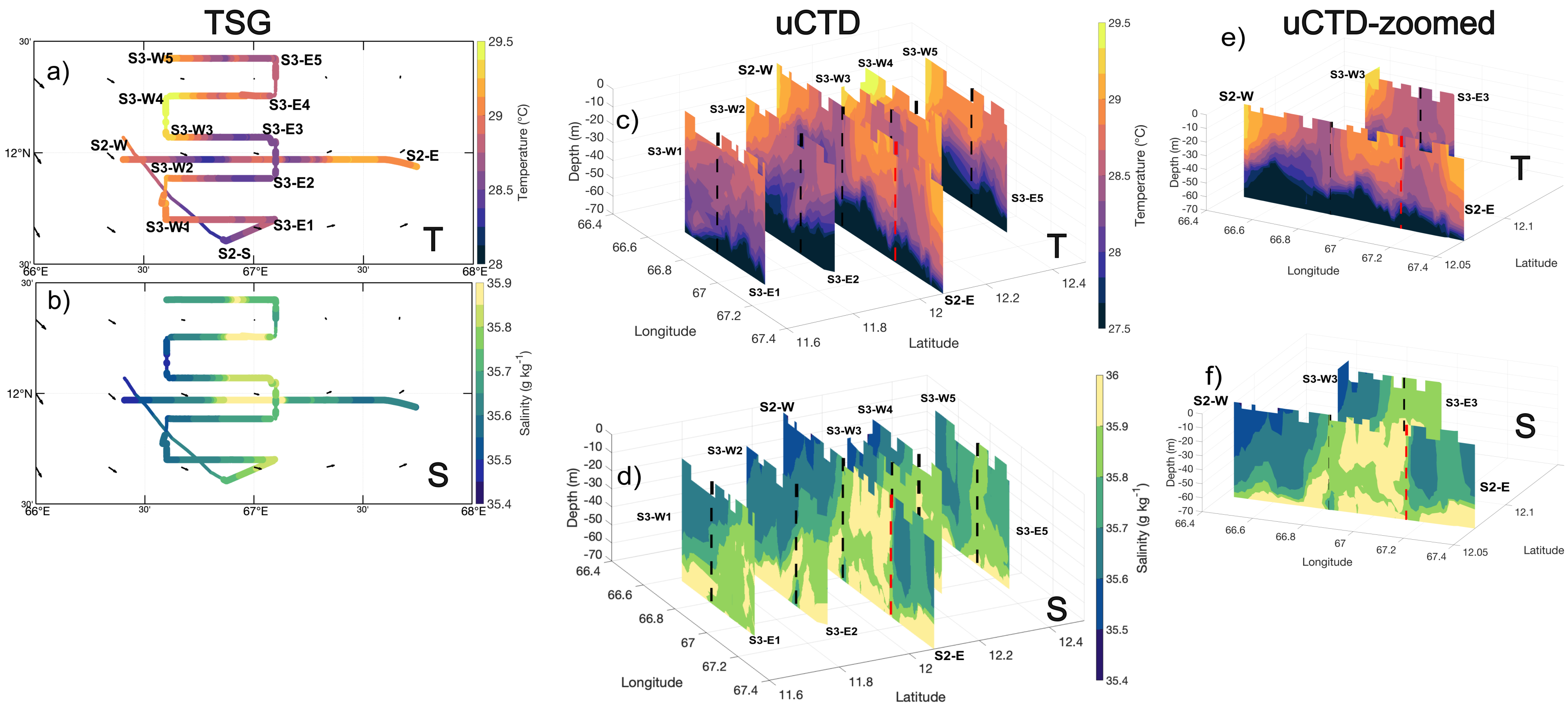

Figure 2. a) Temperature and b) salinity from the ship's TSG during the wake survey. c) Temperature and d) salinity from the uCTD during the wake survey. e) and f) are the same as c) and d) zooming into section S2-E to S2-W and section S3-E3 to S3-W3, respectively. The arrows in panels a) and b) are ocean surface currents from OSCAR (Dohan, 2021). Black dashed lines in panels (c-f) indicate the shift in meridional velocity over the mixed layer, marking the westward edge of the wake (see Figure 3 for more details). The red dashed line in panels (c-f) during the section S2-W to S2-E indicates the eastward edge of the wake. Panels a, c, d, e and f) feature various survey waypoints described in Table S2. NOTE: The section S3-E3 to S3-W3 is on the same latitude as section S2-E to S2-W. For ease of visualization, the section S3-E3 to S3-W3 has been offset northward by 0.1° in panels c-f) while the section S2-W to S2-E has been offset southward by 0.1° in panels a and b.

compared to those in the vicinity of the wake (Figure 2a,b). As a result of these differences, the formation of this wake results in the development of density fronts at its edges. Observations during this survey also reveal the small-scale meridional variability of the wake, highlighting its meandering nature (Figure 2a,b).

The three-dimensional view of the sections additionally reveal significant differences in the mixed layer structure throughout the wake and its vicinity (Figure 2c,d). Given the south-westerly nature of the winds and its orientation with respect to the wake-associated fronts, the presence of EBFs and mixed layer eddies is anticipated. These can potentially influence the upper ocean structure within the wake and its vicinity by causing an asymmetric recovery (Haney et al., 2012). In order to explore the vertical structure further, we focus on the zonal section between the S2-E and S2-W waypoints. This section is the longest and captures both the eastward and westward edges of the wake (other sections only capture the westward edge, Figure 2).

3.2.1 Section between S2-E and S2-W

Sharp contrasts in velocity and salinity define the western and eastern edges of the cyclone wake, both of which are characterized by outcropping isopycnals of higher surface density (Figure 3). Within the wake itself, a mixed layer depth (MLD) of 32 m and a BLT of 12 m is observed (Figure 3a,b). The wake is also associated with weak eastward and northward flow (Figure 3c,d). On the other hand, fresher and warmer waters (thereby lighter waters. Although, the wake is warm during this survey as well. This is because the survey took place during the afternoon, when the wake warms due to the atmospheric heating. This could potentially impact the mixed layer depth in the wake.) are observed around the wake core (Figure 3a,b). The velocities in the vicinity of the wake contrasts sharply with that within the wake (as further discussed below, Figure 3c,d).

The S2-E to S2-W section also reveals an asymmetric nature associated with the wake recovery. To the west of the wake, isopycnals slope downwards to the west. The MLD is slightly shallower (by about 4 m) when compared to within the wake itself (Figure 3a,b). Flow in this region is characterized by weak eastward (around 0.1 $\mathrm{m\,s^{-1}}$) and stronger southward velocities (0.3 $\mathrm{m\,s^{-1}}$). This flow contrasts sharply to the flow within the wake, producing strong horizontal shear at the front (Figure 3c,d).

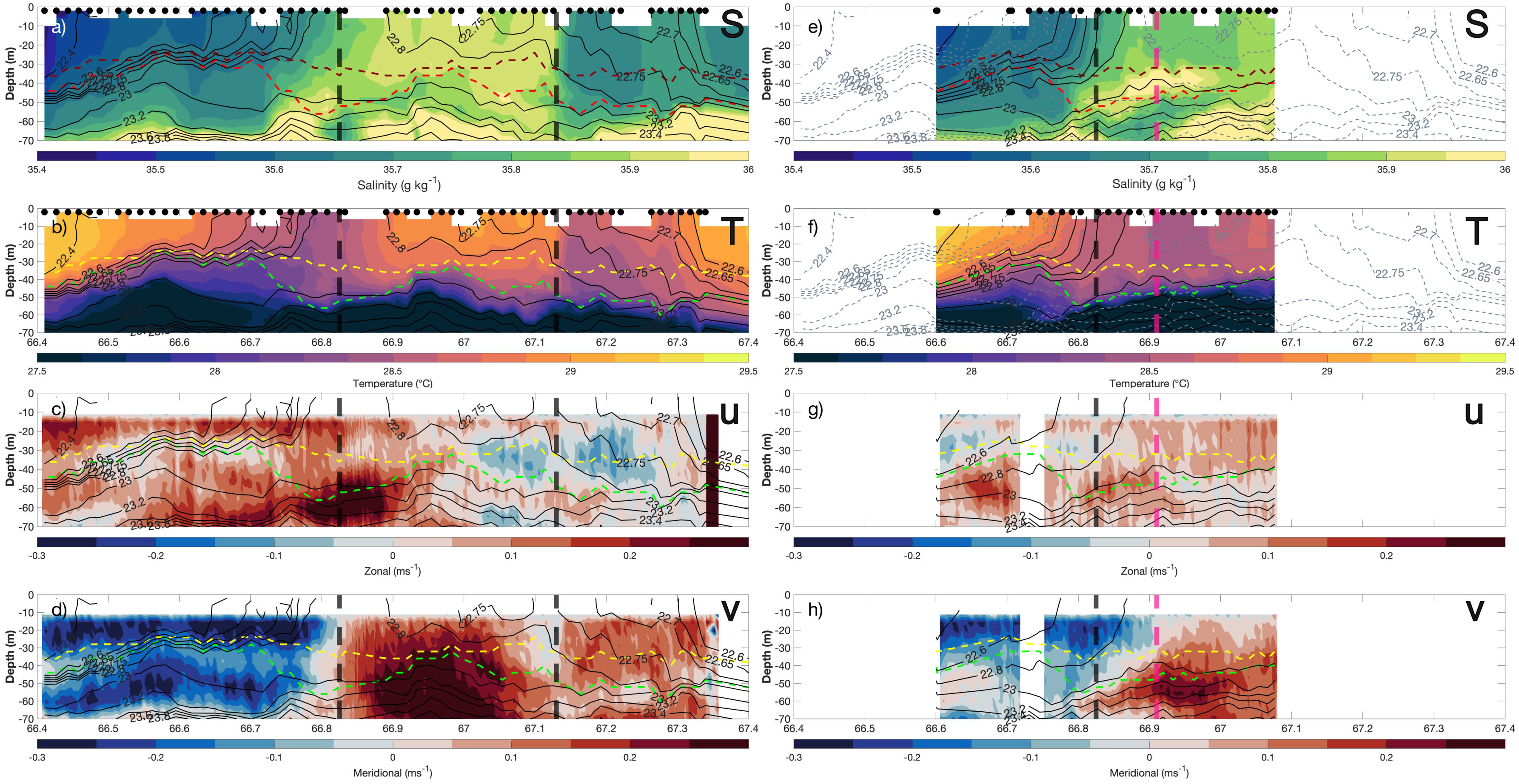

Figure 3. Vertical sections of a) salinity, b) temperature, c) zonal velocity and d) meridional velocity between S2-E and S2-W. The black dots in panels a-b are the individual uCTD profiles. Black contours in each panel indicate the isopycnals. The yellow (dark red in panel a) line in panels b,c,d indicate the MLD while the green (red in panel a) line indicate the ILD. Vertical black dashed lines indicate section dividers based on change in meridional velocity. Panels e-h are the same as a-d except the vertical section is between S3-W3 and S3-E3 (which is a shorter repeat section). The gray lines in panels e) and f) indicate the isopycnals from the original section (panels a and b, respectively). The black dashed line in these panels is the westward edge of the wake in the original section (panels a-d) while the red dashed line is the westward edge of the wake in the S3-W3 and S3-E3 repeat section.

Isopycnals east of the wake are sloping down to the east, with steeper slopes than those observed on the western edge. This region is also characterized by smaller scale features of O(1 km) around 67.2 ° E (Figure 2a,b). The MLD in the eastern edge is deeper (by 9 m), while the BLT is thicker (by 8 m) when compared to within the wake. When compared to the western edge of the wake, the eastern edge has a deeper mixed layer (by about 12 m) and a BLT that is nearly twice as thick. The flow in the eastern edge of the wake is weakly westward and northward. Upon eliminating the effects of the background flow (by subtracting the mean velocities below the mixed layer depth along the whole section), evidence of weak convergence is observed in this area (Figure S4).

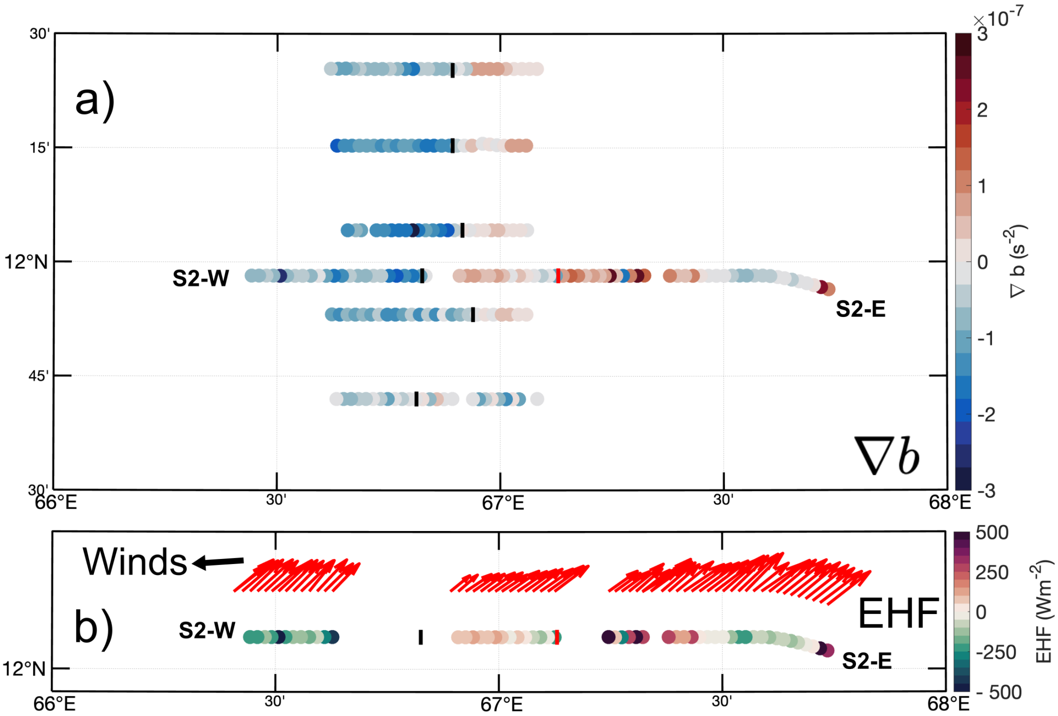

Figure 4. a) Surface buoyancy gradients from the ship's survey in the wake and its vicinity. NOTE: The section S2-E to S2-W is offset by 0.1° to the south as to avoid overlap between repeating sections. b) Ekman heat flux (EHF) in the section S2-W to S2-E. The red arrows indicate concurrent wind directions.

Understanding the buoyancy gradients in the wake is crucial as they serve as reservoirs of potential and kinetic energy, which can catalyze instabilities and impact upper-ocean mixing and stratification (Haine & Marshall, 1998; Ferrari & Wunsch, 2009). The buoyancy gradient values changes signs in section S2-E to S2-W since the denser (i.e. less buoyant) waters within the wake are surrounded by lighter (or more buoyant) waters (Figure 4a). Asymmetry is observed in the surface buoyancy gradients as well, where the peak magnitude of the buoyancy gradient at the eastern edge of the wake (2.5×10^{-7} s^{-2}) is 1.67 times higher than that on the western edge of the wake (1.5×10^{-7} s^{-2}) (Figure 4a). The buoyancy gradients associated with the cyclone wakes are of the same order of magnitude as within submesoscale meanders generated in Gulf Stream (Shcherbina et al., 2015).

Estimates of buoyancy gradients (from uCTD) and south-westerly wind stresses (from ship-based meteorological measurements, Figure 4b) are used to calculate the Ekman buoyancy flux (EBF $= \frac{\tau_y}{\rho_o f}\frac{\partial b}{\partial x}$, where ρ_o is the reference density, f is the coriolis frequency, τ_y is the meridional wind stress while $\frac{\partial b}{\partial x}$ is the horizontal buoyancy gradient in zonal direction). The EBF is converted into equivalent Ekman heat fluxes (EHF $= \frac{(EBF)\rho_o c_p}{\alpha g}$, where c_p is the specific heat of water, α is the thermal expansion coefficient. g is the acceleration due to the gravity). EHF values are found to be of O(500 W/m^2) at both the edges of the wake (Figure 4b), a magnitude which could trigger submesoscale processes like frontal slumping and steepening (D'Asaro et al., 2011; Brannigan et al., 2015). This is further confirmed by calculating the Rossby number and Richardson number throughout the section, where these numbers are O(1) near the edges of the wake (Thomas et al., 2008).

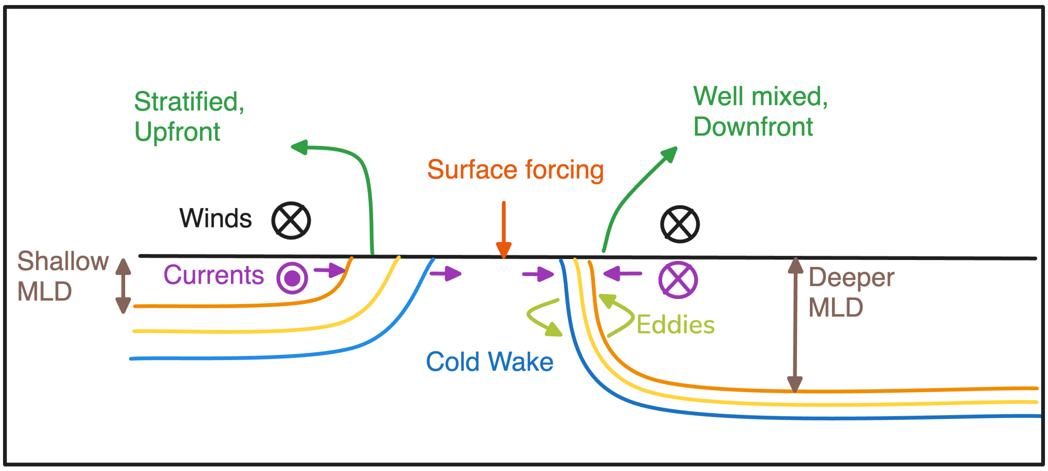

Figure 5. Schematic explaining the forcing conditions and the asymmetric response of the cold wake in section S2-W to S2-E (adapted from Haney et al., 2012)

With respect to the orientation of the winds (Figure 4b) and the density gradients (Figure 3a-d, 4a), the westward edge of the wake has an upfront configuration, while the eastward edge of the wake has a downfront scenario. This explains the asymmetry observed in the vertical structure of the wake, where the west side (forced by upfront winds) is undergoing restratification (and hence shallower MLDs), while the east side (forced by downfront winds) has a stronger buoyancy gradient as a result of destratification (Figure 5). This is consistent the sign of the EHFs, which are stabilizing at the western edge of the wake and are destabilizing at the eastern edge. Despite the destabilizing effect from the EBFs at the eastern edge of the front, the isopycnals are not fully vertical but slope down to the east, indicating ongoing restratification. Previous studies have shown that a front can undergo restratification even with a destratifying downfront configuration in the presence of mixed layer eddies (e.g. Mahadevan et al., 2010). Thus, the restratification at the eastern edge, despite its downfront configuration, provides indirect evidence of the presence of mixed layer eddies.

Using the theoretical scalings derived in Haney et al. (2012), we estimate that the recovery time scales associated with the surface forcing (T_{sf}), EBFs (T_{ebf}) and mixed layer eddies (T_{eddy}) separately to be 29.6 ± 7, 25.4 ± 6 and 38.4 ± 8 days respectively. Thus, EBFs lead to a slightly faster recovery rate (see Supplementary Section S1 for more information on the scaling analysis). However, the combination of surface forcing and EBFs yields an estimated recovery timescale of 9 ± 2 days, while the combination of all of the above processes (including mixed layer eddies) results in an estimated recovery timescale of 7 ± 1 days (Supplementary Section S1). This timescale closely aligns with the observed SST recovery (Figure 1b), however high-resolution numerical simulations are needed to further validate the recovery timescales quoted here. Nonetheless, this scaling analysis highlights that role of lateral processes like EBFs and mixed layer eddies in causing a faster recovery of the wake, underscoring the important role of wind-front coupling in such cases.

3.2.2 Section between S3-E3 and S3-W3: Repeat Section

As mentioned previously, the zonal sections of the in-situ survey highlights slight meridional variations within the wake, thereby revealing the meandering nature of the wake (Figure 2, 4a). The repeat section between S3-E3 and S3-W3 (referred to as the repeat section hereafter) was conducted along the same latitude as the section S2-E to S2-W (original section hereafter, Figure 2, Table S2) nearly 28 hours later, and hence provided an opportunity to understand the variability of the wake.

The repeat section is shorter and hence does not capture the eastward edge of the wake unlike the original section described in Section 3.2.1 (Figure 2, 3e-h). However, the vertical structure of the repeat section is similar to the original section described above. The main difference is that the westward edge of the wake is displaced by 10 km to the east (Figure 3e-h) during the repeat section survey. This displacement could be due to several factors, including Ekman transport due to the south-westerly monsoon winds, advection by the background flow and near-inertial currents. While Ekman transport and advection are plausible causes, the near-inertial currents are less likely since Cyclone Biparjoy was initially a slow-moving cyclone (with translation speed of 1-2 $\mathrm{m\,s^{-1}}$, Figure S1a), resulting in a smaller near-inertial response (Figure S1c, Price, 1981). Near-inertial currents calculated using the slab model (Pollard & Millard, 1970) forced by MERRA-2 reanalysis product (Global Modeling and Assimilation Office (GMAO), 2015) were roughly 0.05 $\mathrm{m\,s^{-1}}$, which is about one-sixth of the observed currents in this section (Figure 3d,h).

4 Summary and Discussions

Cyclone Biparjoy created a cold wake over the Arabian Sea in June 2023. SST began recovering post-cyclone, reaching steady state in 8 days, far more rapidly than the 19-29 days predicted by one-dimensional models forced by winds and surface fluxes (Price et al., 2008; Haney et al., 2012). The scaling of recovery timescales from Haney et al. (2012) using the observed parameters reveals that the Ekman Buoyancy Flux, surface forcing and mixed layer eddies have similar recovery timescales when acting in isolation (25.4 $\pm$ 6, 29.6 $\pm$ 7 and 38.4 $\pm$ 8 days respectively). However, an estimated recovery timescale of 7 days due to the combination of these processes closely matches the recovery timescale observed from satellite SSTs, highlighting the role of submesoscale processes in speeding up the recovery of the wake (Figure 1b).

In-situ observations across the wake reveal its asymmetrical structure during the recovery as a result of presence of Ekman Buoyancy Flux. This is caused due to the imposition of southwesterly winds on the wake, which leads to upfront forcing on the wake's western edge, leading to shallower MLDs and hence restratifying in nature. In contrast, the wake's eastern edge is forced by downfront winds, with deeper MLD and a presumably destratifying nature. However, observations at the eastern edge of the wake indicate a weak restratifying nature, providing indirect evidence of the presence of mixed layer eddies (Fox-Kemper et al., 2008; Mahadevan et al., 2010). The Ekman Buoyancy Flux (O(500

W/m^2)) as well as Rossby and Richardson numbers (both O(1)) associated with the cyclone wake were found to be sufficient to drive submesoscale processes at the edges of the wake as a result of the density gradients and their interaction with the winds. Given that Cyclone Biparjoy was a slow-moving storm, the near-inertial currents were small.

These results present the first in-situ observations of a post-cyclone wake recovery in the Arabian Sea. Our observations emphasize the significance of the interaction between monsoon winds and the underlying three-dimensional submesoscale fronts in shaping the wake of a slow-moving cyclone through Ekman buoyancy fluxes. This contrasts with faster-moving cyclones, where near-inertial currents primarily dominate the wake evolution (Price, 1981). Understanding this recovery and the associated processes is vital, as it can influence ocean heat transport, nutrient availability (Babin et al., 2004), coral health (Dobbelaere et al., 2024), and the predictability of future cyclones and sub-seasonal weather patterns.

5 Data Availability Statement

Data from the instruments are embargoed under agreement between the U.S. and India until 2029 as one step in fostering the international collaboration. This time frame is intended to allow for students and postdoctoral researchers supported under the project to have sufficient time to publish observation-based results. After the embargo period, data may be requested from the corresponding author. The satellite data for AMSR-2 as well as OISST were obtained from `www.remss.com`, while the level-2 products of MODIS-Aqua and VIIRS were obtained from `https://oceancolor.gsfc.nasa.gov/cgi/browse.pl?sen=amod`. OSCAR currents were obtained from `https://podaac.jpl.nasa.gov/dataset/OSCAR_L4_OC_INTERIM_V2.0`.

Acknowledgments

The authors gratefully acknowledge the support of the US Office of Naval Research for the EKAMSAT-ASTraL Department Research Initiative. S. Kerhalkar and A. Tandon received support from N00014-23-1-2054, A. Kannad and J. Sprintall from N00014-23-1-2091, A. Kinsella from N00014-23-1-2471, and C.M. Lee from N00014-23-1-2085. A. Tandon also acknowledges support from N00014-23-1-2473. The authors extend their gratitude to the Captain, crew, and science party of R/V Roger Revelle during the EKAMSAT pilot field campaign for their invaluable assistance with data collection. S. K. acknowledges the support of the Associate Provost's office, University of Massachusetts Dartmouth, through the

Distinguished Doctoral Fellowship. Special thanks to Joaquim Goes, Charles Kovach, and Sherwin Ladner for their assistance in obtaining L-2 satellite images. The authors also thank Elizabeth J. Thompson, Ludovic Bariteau, Byron Blomquist, Chris Fairall and Sergio Pezoa (from NOAA PSL as a part of NOAA Global Ocean Monitoring and Observations program) as well as Joe (Harindra) Fernando, Jay Orson Hyde and Griffin Modjeski (from University of Notre Dame as a part of EKAMSAT-ASTraL) for their role in QC'ing the surface meteorological measurements presented here. Thanks to Eric D'Asaro for insightful discussions. Lastly, this paper is dedicated to the memory of Sean Haney, who would have been happy to see these observations in line with his numerical results.

References

Babin, S., Carton, J., Dickey, T., & Wiggert, J. (2004). Satellite evidence of hurricane-induced phytoplankton blooms in an oceanic desert. *Journal of Geophysical Research: Oceans*, *109*(C3).

Brannigan, L., Marshall, D. P., Naveira-Garabato, A., & Nurser, A. G. (2015). The seasonal cycle of submesoscale flows. *Ocean Modelling*, *92*, 69–84.

Cao, C., De Luccia, F. J., Xiong, X., Wolfe, R., & Weng, F. (2013). Early on-orbit performance of the visible infrared imaging radiometer suite onboard the Suomi National Polar-Orbiting Partnership (S-NPP) satellite. *IEEE Transactions on Geoscience and Remote Sensing*, *52*(2), 1142–1156.

Cornillon, P., Stramma, L., & Price, J. F. (1987). Satellite measurements of sea surface cooling during hurricane Gloria. *Nature*, *326*(6111), 373–375.

D'Asaro, E. A. (2003). The ocean boundary layer below Hurricane Dennis. *Journal of Physical Oceanography*, *33*(3), 561–579.

D'Asaro, E. A., Sanford, B., Niiler, P. P., & Terrill, E. J. (2007). Cold wake of hurricane Frances. *Geophysical Research Letters*, *34*(15).

Dobbelaere, T., Dekens, A., Saint-Amand, A., Alaerts, L., Holstein, D. M., & Hanert, E. (2024). Hurricanes enhance coral connectivity but also superspread coral diseases. *Global Change Biology*, *30*(6), e17382.

Dohan, K. (2021). *Ocean Surface Current Analyses Real-time (OSCAR) Surface Currents - Near Real Time 0.25 Degree (Version 2.0).* NASA Physical Oceanography Distributed Active Archive Center. Retrieved from `https://podaac.jpl.nasa.gov/dataset/OSCAR_L4_OC_NRT_V2.0` doi: 10.5067/OSCAR-25N20

D'Asaro, E., Lee, C., Rainville, L., Harcourt, R., & Thomas, L. (2011). Enhanced turbulence and energy dissipation at ocean fronts. *science*, *332*(6027), 318–322.

Emanuel, K. (2001). Contribution of tropical cyclones to meridional heat transport by the oceans. *Journal of Geophysical Research: Atmospheres*, *106*(D14), 14771–14781.

Emanuel, K. (2003). Tropical cyclones. *Annual review of earth and planetary sciences*, *31*(1), 75–104.

Evan, A. T., & Camargo, S. J. (2011). A climatology of Arabian Sea cyclonic storms. *Journal of climate*, *24*(1), 140–158.

Ferrari, R., & Wunsch, C. (2009). Ocean circulation kinetic energy: Reservoirs, sources, and sinks. *Annual Review of Fluid Mechanics*, *41*(1), 253–282.

Fox-Kemper, B., Ferrari, R., & Hallberg, R. (2008). Parameterization of mixed layer eddies. Part I: Theory and diagnosis. *Journal of Physical Oceanography*, *38*(6), 1145–1165.

Global Modeling and Assimilation Office (GMAO). (2015). *MERRA-2 tavg1_2d_lnd_Nx: 2d,1-Hourly,Time-Averaged,Single-Level,Assimilation,Land Surface Diagnostics V5.12.4.* Greenbelt, MD, USA, Goddard Earth Sciences Data and Information Services Center (GES DISC). (Accessed: [January 29 2024]) doi: 10.5067/RKPHT8KC1Y1T

Gutiérrez Brizuela, N., Alford, M. H., Xie, S.-P., Sprintall, J., Voet, G., Warner, S. J., ... Moum, J. N. (2023). Prolonged thermocline warming by near-inertial internal waves in the wakes of tropical cyclones. *Proceedings of the National Academy of Sciences*, *120*(26), e2301664120.

Haine, T. W., & Marshall, J. (1998). Gravitational, symmetric, and baroclinic instability of the ocean mixed layer. *Journal of physical oceanography*, *28*(4), 634–658.

Haney, S., Bachman, S., Cooper, B., Kupper, S., McCaffrey, K., Van Roekel, L., ... Ferrari, R. (2012). Hurricane wake restratification rates of one-, two-and three-dimensional processes. *Journal of Marine Research*, *70*(6), 824–850.

IMD. (2023). *Extremely Severe Cyclonic Storm "BIPARJOY" over the ARABIAN Sea (6^{th}-19^{th} June, 2023): A Report.*

Johnston, T. S., Rudnick, D. L., Brizuela, N., & Moum, J. N. (2020). Advection by the North Equatorial Current of a cold wake due to multiple typhoons in the western Pacific: Measurements from a profiling float array. *Journal of Geophysical Research: Oceans*, *125*(4), e2019JC015534.

Johnston, T. S., Wang, S., Lee, C.-Y., Moum, J. N., Rudnick, D. L., & Sobel, A. (2021). Near-inertial wave propagation in the wake of super typhoon mangkhut: Measurements from a profiling float array. *Journal of Geophysical Research: Oceans*, *126*(2), e2020JC016749.

Karnauskas, K. B., Zhang, L., & Emanuel, K. A. (2021). The feedback of cold wakes on tropical cyclones. *Geophysical Research Letters*, *48*(7), e2020GL091676.

Krishnamurti, T., Ardanuy, P., Ramanathan, Y., & Pasch, R. (1981). On the onset vortex of the summer monsoon. *Monthly Weather Review*, *109*(2), 344–363.

Krishnamurti, T., Chakraborty, A., Krishnamurti, R., Dewar, W. K., & Clayson, C. A. (2007). Passage of intraseasonal waves in the subsurface oceans. *Geophysical research letters*, *34*(14).

Levitus, S. (1983). Climatological atlas of the world ocean. *Eos, Transactions American Geophysical Union*, *64*(49), 962–963.

Mahadevan, A., Tandon, A., & Ferrari, R. (2010). Rapid changes in mixed layer stratification driven by submesoscale instabilities and winds. *Journal of Geophysical Research: Oceans*, *115*(C3).

Mei, W., & Pasquero, C. (2012). Restratification of the upper ocean after the passage of a tropical cyclone: A numerical study. *Journal of physical oceanography*, *42*(9), 1377–1401.

Monterey, G. I., & Levitus, S. (1997). Seasonal variability of mixed layer depth for the world ocean.

Mrvaljevic, R. K., Black, P. G., Centurioni, L. R., Chang, Y.-T., D'Asaro, E. A., Jayne, S. R., ... others (2013). Observations of the cold wake of Typhoon Fanapi (2010). *Geophysical Research Letters*, *40*(2), 316–321.

NASA Goddard Space Flight Center, O. B. P. G. (2018). *Moderate-resolution Imaging Spectroradiometer (MODIS) Aqua Ocean Color Data* [dataset]. NASA OB.DAAC. Retrieved from `https://oceancolor.gsfc.nasa.gov/data/10.5067/AQUA/MODIS/L2/OC/2018/` doi: 10.5067/AQUA/MODIS/L2/OC/2018

Pasquero, C., & Emanuel, K. (2008). Tropical cyclones and transient upper-ocean warming. *Journal of Climate*, *21*(1), 149–162.

Pinkel, R. (2012). Velocity imprecision in finite-beamwidth shipboard Doppler sonar:

A first-generation correction algorithm. *Journal of Atmospheric and Oceanic Technology*, *29*(10), 1569–1580.

Pollard, R. T., & Millard, R. (1970). Comparison between observed and simulated wind-generated inertial oscillations. In *Deep sea research and oceanographic abstracts* (Vol. 17, pp. 813–821).

Price, J. F. (1981). Upper ocean response to a hurricane. *Journal of Physical Oceanography*, *11*(2), 153–175.

Price, J. F., Morzel, J., & Niiler, P. P. (2008). Warming of SST in the cool wake of a moving hurricane. *Journal of Geophysical Research: Oceans*, *113*(C7).

Reynolds, R. W., Smith, T. M., Liu, C., Chelton, D. B., Casey, K. S., & Schlax, M. G. (2007). Daily high-resolution-blended analyses for sea surface temperature. *Journal of climate*, *20*(22), 5473–5496.

Sanabia, E. R., & Jayne, S. R. (2020). Ocean observations under two major hurricanes: Evolution of the response across the storm wakes. *AGU Advances*, *1*(3), e2019AV000161.

Shcherbina, A. Y., Sundermeyer, M. A., Kunze, E., D'Asaro, E., Badin, G., Birch, D., ... others (2015). The LatMix summer campaign: Submesoscale stirring in the upper ocean. *Bulletin of the American Meteorological Society*, *96*(8), 1257–1279.

Smith, T. A., Jolliff, J. K., Walker, N. D., & Anderson, S. (2019). Biophysical Submesoscale Processes in the Wake of Hurricane Ivan: Simulations and Satellite Observations. *Journal of Marine Science and Engineering*, *7*(11), 378.

Stramma, L., Cornillon, P., & Price, J. F. (1986). Satellite observations of sea surface cooling by hurricanes. *Journal of Geophysical Research: Oceans*, *91*(C4), 5031–5035.

Thomas, L. N., Tandon, A., & Mahadevan, A. (2008). Submesoscale processes and dynamics. *Ocean modeling in an Eddying Regime*, *177*, 17–38.

Vincent, E. M., Lengaigne, M., Madec, G., Vialard, J., Samson, G., Jourdain, N. C., ... Jullien, S. (2012). Processes setting the characteristics of sea surface cooling induced by tropical cyclones. *Journal of Geophysical Research: Oceans*, *117*(C2).

Wentz, F., Meissner, T., Gentemann, C., Hilburn, K., & Scott, J. (2014). *Remote Sensing Systems GCOM-W1 AMSR2 3-Day Environmental Suite on 0.25 deg* *grid, Version 08.2* [dataset]. Remote Sensing Systems, Santa Rosa, CA. Retrieved from `www.remss.com/missions/amsr`

Yi, Z., Qiu, C., Wang, D., Cai, Z., Yu, J., & Shi, J. (2024). Submesoscale kinetic energy induced by vertical buoyancy fluxes during the tropical cyclone Haitang. *Journal of Geophysical Research: Oceans*, *129*(7), e2023JC020494.